J Mol Med (2013) 91:825–837
DOI 10.1007/s00109-013-1006-4

JMolMed

ORIGINAL ARTICLE

Functional expression of Rab escort protein 1 following AAV2-mediated gene delivery in the retina of choroideremia mice and human cells ex vivo

Tanya Tolmachova · Oleg E. Tolmachov · Alun R. Barnard · Samantha R. de Silva · Daniel M. Lipinski · Nathan J. Walker · Robert E. MacLaren · Miguel C. Seabra

Received: 29 September 2012 / Revised: 23 January 2013 / Accepted: 31 January 2013 / Published online: 12 June 2013

Abstract Choroideremia (CHM) is an X-linked retinal degeneration of photoreceptors, the retinal pigment epithelium (RPE) and choroid caused by loss of function mutations in the *CHM*/*REP1* gene that encodes Rab escort protein 1. As a slowly progressing monogenic retinal degeneration with a clearly identifiable phenotype and a reliable diagnosis, CHM is an ideal candidate for gene therapy. We developed a serotype 2 adeno-associated viral vector AAV2/2-CBA-REP1, which expresses REP1 under control of CMV-enhanced chicken β-actin promoter (CBA) augmented by a Woodchuck hepatitis virus post-transcriptional regulatory element. We show that the AAV2/2-CBA-REP1 vector provides strong and functional transgene expression in the D17 dog osteosarcoma cell line, CHM patient fibroblasts and CHM mouse RPE cells in vitro and in vivo. The ability to transduce human photoreceptors highly effectively with this expression cassette was confirmed in AAV2/2-CBA-GFP transduced human retinal explants ex vivo. Electroretinogram (ERG) analysis of AAV2/2-CBA-REP1 and AAV2/2-CBA-GFP-injected wild-type mouse eyes did not show toxic effects resulting from REP1 overexpression. Subretinal injections of AAV2/2-CBA-REP1 into CHM mouse retinas led to a significant increase in a- and b-wave of ERG responses in comparison to sham-injected eyes confirming that AAV2/2-CBA-REP1 is a promising vector suitable for choroideremia gene therapy in human clinical trials.

Keywords Rab escort protein 1 · Gene therapy · Choroideremia · Rab GTPase · Retinitis pigmentosa · AAV

Introduction

Choroideremia (CHM) is an X-linked retinal degeneration of choroid, photoreceptors and retinal pigment epithelium (RPE) affecting approximately one in 50,000 patients worldwide [1]. CHM is caused by the loss of function mutations in the *CHM*/*REP1* gene (Xq21.2) that encodes Rab escort protein 1 (REP1) [2, 3]. First symptoms, such as night blindness and constriction of visual field, appear in young male patients and slowly progress towards complete blindness by the fifth decade. The pathogenesis of the disease is complex, involving degeneration of photoreceptors and RPE, followed ultimately by extreme thinning of the choroid [4, 5].

REP1 is important for the function of Rab proteins, which are small Ras-related GTPases [6]. Rabs regulate intracellular vesicular transport through association with intracellular membranes via one or two prenyl groups and

Electronic supplementary material The online version of this article (doi:10.1007/s00109-013-1006-4) contains supplementary material, which is available to authorized users.

T. Tolmachova · O. E. Tolmachov · M. C. Seabra (✉)
Molecular Medicine Section, National Heart and Lung Institute, Imperial College London, London SW7 2AZ, UK
e-mail: m.seabra@imperial.ac.uk

A. R. Barnard · S. R. de Silva · D. M. Lipinski · N. J. Walker · R. E. MacLaren
Nuffield Laboratory of Ophthalmology, University of Oxford and Oxford Eye Hospital NIHR Biomedical Research Centre, Oxford OX3 9DU, UK

N. J. Walker · R. E. MacLaren (✉)
Moorfields Eye Hospital, UCL Institute of Ophthalmology NIHR Biomedical Research Centre, London EC1V 9EL, UK
e-mail: enquiries@eye.ox.ac.uk

interaction with the effectors, which is dependent on conformational changes induced by GDP/GTP binding [7]. Together with Rab geranylgeranyl transferase, REP1 and its homologue REP2 participate in prenylation of Rabs and thus are vital for the functionality of Rabs [8]. REP2 (encoded by the *CHML* gene) is a close homologue of REP1, which can compensate for the loss of REP1 in most human tissues except the eye [9].

As a slowly progressing monogenic disorder, CHM is potentially treatable by gene addition therapy. RPE and photoreceptors are the layers that degenerate first in CHM with deterioration of choroid at the later stages; thus, the optimal gene therapy vector is required to target RPE and photoreceptors at the first instance. In our previous work, we generated a conditional mouse knockout and showed that both RPE and photoreceptors degenerate independently [5]. Similarly, pathological specimens from humans have shown evidence for independent degeneration of rod photoreceptors over focal regions where RPE appears normal [4, 10]. At the same time, the rate of photoreceptor degeneration is enhanced when the REP1 is ablated in both layers [5]. In our previous work, we showed that a lentiviral vector pseudotyped with vesicular stomatitis virus protein G provided strong and stable expression of the human *CHM*/*REP1* cDNA transgene in human and mouse choroideremia cells, including RPE, which resulted in an increase of prenylation activity [11]. However, lentiviral vectors were not optimal for CHM treatment because transduction of the neuroretina was limited to the injection site.

With a functional fovea, safety with regard to avoiding a vector-related inflammatory reaction is of paramount importance. Two recent clinical trials had demonstrated that serotype 2 adeno-associated viral (AAV2) vectors have no long-term retinal toxicity when administered at the dose range 10^{10}–10^{11} genome particles [12, 13]. Importantly, in addition to transducing the RPE, AAV2 is also known to target rod photoreceptors efficiently in the non-human primate [14], providing the ideal tropism for a CHM gene therapy strategy.

The aim of our study was to develop and test a suitable AAV-based vector with *CHM*/*REP1* cDNA transgene for future CHM clinical trials. Specifically, we wished to optimise the expression cassette of AAV2 so that we could enhance the level of gene expression in photoreceptors without increasing the overall dose of viral vector particles, which might have a negative effect on patients who still have a fully functional fovea.

Materials and methods

Mice

All animals used in this study were treated humanely in accordance with the UK Home Office Regulations under project licences 70/6176 and 70/7078. Mice were maintained on a 12:12-h light/dark cycle. $Chm^{Null/WT}$ mice are carrier females with choroideremia phenotype; these animals were described in detail previously [15].

Construction and production of AAV vectors

Human *CHM*/*REP1* cDNA was obtained from Frans Cremers (Nijmegen Centre for Molecular Life Sciences, Netherlands) and modified by the insertion of a Kozak consensus sequence at the 5′-end. To generate pAAV2-EFS-GFP and pAAV2-EFS-REP1, AAV backbone vector plasmid pAAV-MCS was obtained from Stratagene as a part of the AAV Helper-Free System. Plasmid pAAV2-MCS contains 5′ and 3′ AAV2 inverted terminal repeats (ITRs), CMV promoter, β-globin intron and human growth hormone polyadenylation site. CMV promoter and β-globin intron of pAAV-MCS were removed and replaced with the EFS-*EGFP* or EFS-*CHM*/*REP1* cDNA cassette that was excised from pWPT-GFP and pWPT-REP1, respectively [11]. EFS is a short version of elongation factor 1-α promoter. The Woodchuck hepatitis virus post-transcriptional regulator element (WPRE) was excised from the plasmid pWPI (http://www.addgene.org) and inserted downstream of the transgene (*EGFP* or *CHM*/*REP1* cDNA).

The pAAV2-CBA-GFP and pAAV2-CBA-REP1 vector contained 5′ and 3′ ITRs, cytomegalovirus (CMV) enhanced chicken β-actin (CBA) hybrid promoter, a modified WPRE and bovine growth hormone polyadenylation sequence. The modified WPRE included deletion of the We2 promoter/enhancer and mutation of the We1 promoter [16] to prevent expression of the viral X antigen [17]; the sequence was previously used in patients in a US Food and Drug Administration (FDA)-approved gene therapy clinical trial for Parkinson's disease [18].

All viral batches were generated by Gene Detect (Auckland, New Zealand) in order to use an optimised protocol and purification steps that could be scaled up for good medical practice vector production at a later date. This ensured that the final vector suspension matched as closely as possible the product that would be used for a future clinical trial. Plasmids pAAV2-EFS-GFP and pAAV2-EFS-REP1 were used to produce AAV vector virions of serotype 2 (AAV2/2-EFS-GFP and AAV2/2-EFS-REP1) and 5 (AAV2/5-EFS-GFP and AAV2/5-EFS-REP1). Vectors pAAV2-CBA-GFP and pAAV2-CBA-REP1 were used to produce AAV vectors of serotype 2 (AAV2/-CBA-GFP and AAV2/2-CBA-REP1). Titres (genomic particles per millilitre) were AAV2/2-EFS-GFP (1.2×10^{12}), AAV2/5-EFS-GFP (1.0×10^{12}), AAV2/2-EFS-REP1 (1.4×10^{12}), AAV2/5-EFS-REP1 (1.0×10^{12}), AAV2/2-CBA-GFP (1.1×10^{12}) and AAV2/2-CBA-REP1 (1.1×10^{12}).

Transduction of the cultured cells

Dog osteosarcoma D17 cells were cultured in Dulbecco's modified Eagle's medium (DMEM) supplemented with 10 % foetal bovine serum (FBS). Human CHM fibroblasts with full deletion of *CHM/REP1* gene and control fibroblasts were obtained from Ian MacDonald (University of Alberta, Canada). CHM and control fibroblasts were cultured in DMEM/F12+15 % FBS+2 mM L-glutamine + penicillin/streptomycin. Prior to transduction cells were plated into 12-well dish (D17 cells at 7.5×10^4 cells per well and CHM cells at 3×10^4 cells per well). The next day medium was removed, cells were washed with PBS and 1 ml of Iscove's modified Dulbecco's medium (IMDM) supplemented with 10 mM hydroxyurea was added to the wells for overnight treatment. Cells were washed with IMDM twice, and 0.5 ml of IMDM + viral vector (10^9 gp) was added to the cells for 2 h, followed by addition of 0.5 ml of IMDM+20 % FBS.

Immunoblotting and in vitro prenylation assay

The protocol for immunoblotting has been described previously [11]. Antibodies used in the current study were: mouse monoclonal 2F1 (specific for human REP1, dilution 1:1,000); rabbit serum J905 (pan-REP, specific for mouse, rat and human isoforms of REP1 and REP2); mouse monoclonal α-tubulin (Sigma, dilution 1:5,000) and mouse monoclonal anti-GFP (Zymed, dilution 1:2,000). Quantification of western blots was performed with ImageJ software. Plots show Optical Density and Relative Density (%) which is Optical Density normalised to α-tubulin signal in the same lane (Relative Density=Optical Density× 100/Optical Density for α-tubulin). The in vitro prenylation assay was performed on cytosolic fractions of tissue and cell lysates that were collected after ultracentrifugation (100,000×*g*, 1 h, 4 °C) as described in [11]. Quantification of the exposed film was performed with ImageJ software.

Cultures of ex vivo retinal transplants

UK Research Ethics Committee (REC) approval was obtained to culture samples of retina ex vivo from patients undergoing retinectomy for complex retinal detachment surgery (REC reference no. 10/H0505). A 23-gauge pars plana vitrectomy was performed for complex retinal detachment surgery which required removal of retinal tissue inferiorly (retinectomy). Discs of the retina were cut with the vitrectomy system at a slow rate of 60 cuts/min (Ocutome; Alcon Surgical, Irvine, TX, USA), refluxed into the eye, aspirated with a flute needle and placed in balanced salt solution. Within 1 h of removal from the eye, the retinectomy samples were transferred using a 5-ml pipette into four organotypic culture inserts (cat. no. 353095; BD Falcon, Bedford, MA, USA) and placed in a 24-well plate. Samples were cultured in 700 μl of culture media containing Neurobasal A, L-glutamine (0.08 mM), penicillin (100 U/ml), streptomycin (100 U/ml), B27 supplement (2 %) and N2 supplement (1 %), all obtained from Invitrogen Ltd., Paisley, UK [19]. Explants were maintained at 34 °C in a 5 % CO_2 environment. After 24 h, medium was changed and 10 μl of AAV2/2-CBA-GFP (titre 1×10^{12} gp/ml) was added to each well, with two wells tested per virus. Culture medium was changed every 48 h, and explants were imaged daily on an inverted epifluorescence microscope (DMIL; Leica, Wetzlar, Germany). Explants were fixed 11 days post-transduction in 4 % paraformaldehyde overnight, cryoprotected in 20 % sucrose for 1 h, embedded in OCT compound (Tissue-Tek, Sakura Finetek, the Netherlands) and frozen on dry ice. Explants were cut into 16 μm, counterstained with anti-recoverin primary antibody (Millipore, dilution 1:1,000), secondary Alexa 633 (Invitrogen, dilution 1:300) and DAPI (ProLong Gold antifade reagent with DAPI, Invitrogen, Paisley, UK) and viewed on a confocal microscope (LSM710; Zeiss, Jena, Germany). The retinal explant in Fig. 4 was from a 40-year-old gentleman who required retinectomy for chronic retinal detachment following endogenous Klebsiella endophthalmitis. A similar transduction pattern with the vector was also seen in a retinal explant sample from a 60-year-old lady who required retinectomy for a chronic retinal detachment with proliferative vitreoretinopathy that had previously been treated with vitrectomy, silicone oil and scleral buckle.

Subretinal injections and morphological study

Mice were anaesthetised with a mixture of Domitor/ketamine; pupils were dilated with phenylephrine hydrochloride (2.5 %) and tropicamide (1 %). Proxymetacaine hydrochloride (0.5 %) eye drops were used for additional local anaesthesia; carbomer gel (Viscotears, Novartis Pharmaceuticals Ltd) and a small circular glass coverslip were used to achieve good visualisation of the fundus. The injection was performed through posterior retina using 10-μl Hamilton syringe and a pointed 34G needle. Mouse eyes for histology were fixed in 4 % paraformaldehyde for 1 h. Samples were cryoprotected in 20 % sucrose overnight and embedded in the OCT compound (BDH Poole, Dorset, UK). Sections were cut at 7 μm thickness, air-dried, covered with mounting media Prolong Gold and examined under a Zeiss LSM-510 inverted confocal microscope.

ERG analysis

Before the electroretinogram (ERG) procedure, mice were dark adapted (>1 h), and experimental preparation was performed under dim red illumination. The mice were anaesthetised with a single intraperitoneal injection of

medetomidine hydrochloride (Domitor; 1 mg/kg body weight) and ketamine (60 mg/kg body weight) in water. The pupils were dilated using 1 % tropicamide eye drops. ERGs were recorded using an electroretinography console (Espion E2; Diagnosys LLC, Cambridge, UK) that also generated and controlled the light stimulus. Single-flash stimuli were delivered in a Ganzfeld dome with the intensity increasing from −6 to 1 log cds/m^2 in log unit steps. For dim stimuli (−6 and −5 log cds/m^2), 20 responses were averaged with an interstimulus interval (ISI) of 2 s. For stimuli of −4 and −3 log cds/m^2, 20 responses were averaged with an ISI of 5 s; for stimuli of −2 and −1 log cds/m^2, ten responses were averaged with an ISI of 10 s. For bright stimuli (0 and 1 log cds/m^2), five responses were averaged with an ISI of 20 s. After dark-adapted recordings were completed, animals were exposed to a full field 30 cd/m^2 white background for 10 min. Light-adapted ERGs were then recorded in response to a bright white stimulus (1 log cds/m^2, 20 responses averaged, ISI=500 ms) superimposed on the constant background. ERGs were recorded from both eyes simultaneously using custom-made active electrodes (platinum wire loop type) positioned concentrically to the cornea using micromanipulators. Hypromellose eye drops (0.5 % methylcellulose solution) were used to provide good electrical contact and to maintain corneal moisture. A reference electrode (subcutaneous stainless steel needle) was placed in the scruff, and an identical ground electrode was positioned at the base of the tail. All recordings were made in a custom-made, light-tight Faraday cage. Signals were differentially amplified and digitized at a rate of 5 kHz. Amplitudes of the major ERG components (a- and b-waves for dark-adapted, b-wave only for light-adapted) were measured (Espion software; Diagnosys LLC) using automated and manual methods.

Results

Generation of AAV viral vectors

As a candidate promoter, we tested two ubiquitous promoters that were shown to be active in RPE and photoreceptors: elongation factor 1-α promoter (shortened version, EFS) and CMV-enhanced chicken β-actin promoter (CBA) [20, 21]. As a therapeutic gene, we used *CHM*/*REP1* cDNA with an upstream Kozak sequence that was previously shown to be functionally expressed from the lentiviral backbone [11]; the *EGFP* gene was employed as a control transgene (Fig. 1a). To enhance transgene expression, all vectors contained a WPRE next to the 3′-end of the transgene followed by a polyadenylation signal site. EFS and CBA plasmids carrying *CHM*/*REP1* cDNA or EGFP transgene were used to generate AAV vectors of serotype 2 and serotype 5 that were previously shown to transduce RPE and photoreceptors [22].

Expression of CHM/REP1 cDNA and EGFP transgenes in D17 cells

Initially, the AAV2/2-EFS-GFP, AAV2/5-EFS-GFP and AAV2/2-CBA-GFP vectors were tested by transduction of dog osteosarcoma D17 cells. Expression of GFP was detected 2 days post-transduction (P0) by FACS (Fig. 1b) and immunoblotting using anti-GFP antibody (Fig. 1c, d). The cells were passaged and expression was tested after 6 days (8 days post-transduction, P1) and then 4 days after the second passage (12 days post-transduction, P2). Transduction rate (percentage of GFP-positive cells at P0) was similar for AAV2/2-EFS-GFP and AAV2/2-CBA-GFP (17.7 and 17.3 %, respectively) and lower (12.5 %) for AAV2/5-EFS-GFP (Fig. 1b). The prevalence of GFP-expressing cells decreased with each passage for all three vectors (at P1: 9.2 % for AAV2/2-EFS-GFP, 9.1 % for AAV2/2-CBA-GFP, 8 % for AAV2/5-EFS-GFP), which is consistent with the episomal non-replicating status of the AAV vector and proportional decrease in copy number with each cell division (Fig. 1b). Western blot analysis showed robust transgene expression from both EFS and CBA promoters, with expression from CBA being slightly higher than from EFS: 150 and 107 %, respectively, at P0, 139 and 102 % at P1 and 33 and 21 % at P2 (Fig. 1d).

Having optimised the viral transduction using the GFP reporter, we transduced D17 cells with AAV2/2-EFS-REP1, AAV2/5-EFS-REP1 and AAV2/2-CBA-REP1 vectors carrying the *CHM*/*REP1* cDNA transgene, and the amount of REP1 was detected by immunoblotting using 2F1 antibody specific for human REP1 2 days post-transduction (Fig. 1e). Unlike GFP, expression of REP1 from the CBA promoter was considerably stronger than from the EFS promoter: 156.5 versus 26.9 % for AAV2/2-EFS-REP1 and 23.8 % for AAV2/5-EFS-REP1 (Fig. 1f).

Thus, our data show that viral vectors of both serotypes (2 and 5) were able to transduce D17 cells. As expected, expression of both transgenes (*CHM*/*REP1* and *EGFP*) in D17 cells was transient due to the episomal status of the vector. Expression from both EFS and CBA promoters was detected as early as 2 days post-transduction and was higher from CBA promoter than from EFS (especially for the *CHM*/*REP1* transgene).

Expression of CHM/REP1 cDNA and EGFP transgenes in CHM fibroblasts

To confirm that *CHM*/*REP1* transgene expression is not impaired in CHM cells, we used fibroblasts from a CHM patient with full deletion of the *CHM*/*REP1* gene [23]. CHM fibroblasts were transduced with AAV2/2-EFS, AAV2/5-EFS and AAV2/2-CBA vectors carrying *EGFP* or *CHM*/*REP1* cDNA transgenes. Expression was detected by immunoblotting using

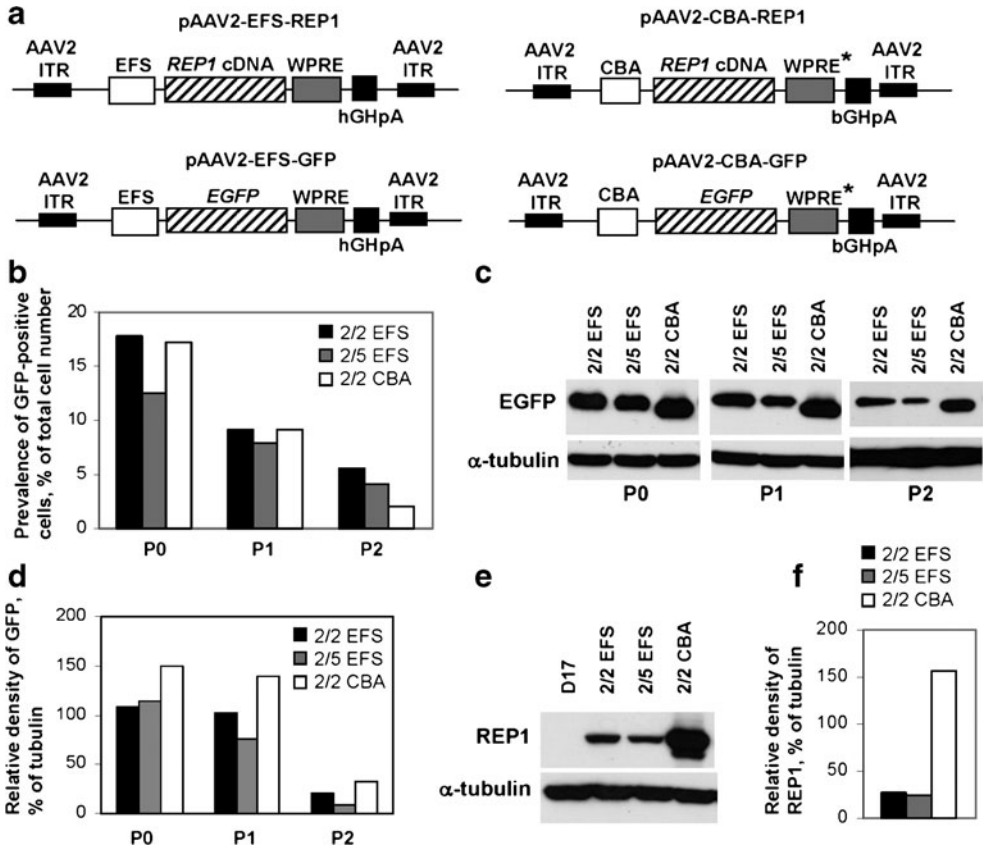

Fig. 1 Expression of *CHM*/*REP1* cDNA and *EGFP* transgenes in dog D17 cell line. **a** Plasmids pAAV2-EFS-REP1 and pAAV2-CBA-REP1 carry the *CHM*/*REP1* cDNA transgene with Kozak sequence at the 5′-end. Plasmids pAAV2-EFS-GFP and pAAV2-CBA-GFP were used to generate control viral vectors. WPRE* is a WPRE that has been modified by deleting the We2 promoter/enhancer and mutating the We1 promoter (for other details, see "Materials and methods"). **b**–**d** D17 cells were transduced with AAV2/2-EFS-GFP, AAV2/5-EFS-GFP and AAV2/2-CBA-GFP. Expression of GFP was analysed 2 days post-transduction (P0). Cells were replated, cultured for additional 6 days and analysed (P1), then replated and analysed after 4 days in culture (P2). **b** FACS analysis shows prevalence of transduced cells (% of total cell number). **c** Immunoblot analysis of the total protein lysate using GFP antibody and α-tubulin antibody as a loading control. **d** Quantification of the western blot shown in **c** using ImageJ software. Data are presented as relative density of GFP signal in relation to α-tubulin signal. **e** Immunoblot analysis of the D17 cells transduced with AAV2/2-EFS-REP1, AAV2/5-EFS-REP1 and AAV2/2-CBA-REP1 using 2F1 antibody specific for human REP1 and α-tubulin antibody as a loading control. Cells were analysed 48 h post-transduction. **f** Quantification of the western blot shown in **e** using ImageJ software. Data are presented as relative density of GFP signal in relation to α-tubulin signal

an anti-GFP antibody (Fig. 2a) and anti-human REP1 antibody (Fig. 2b). For both EGFP and REP1, expression levels were significantly higher with the CBA promoter in comparison to EFS.

Our results identified that the CBA promoter provided a considerably higher level of expression in CHM cells. To measure level of CBA-driven expression of REP1 in transduced cells in comparison to endogenous REP1 in control wild-type (WT) fibroblasts, we transduced human CHM fibroblasts with AAV2/2-CBA-REP1 and compared amount of REP1 using 2F1 antibody (Fig. 2c). Quantification of the western blot showed that the intensity of the REP1-specific band in 40 μg of WT lysate was roughly equal to the intensity of REP1 band in 5 μg of lysate from transduced cells (CHM AAV2/2-CBA-REP1) (Fig. 2d). Thus, the level of expression of REP1 protein under these conditions was approximately eight times higher than endogenous REP1 in control fibroblasts, confirming that the REP1 defect does not prevent successful AAV2/2-mediated transduction and transgene expression.

The functionality of the REP1 transgene was tested by an in vitro prenylation assay in CHM fibroblasts and D17 cells (Fig. 2e, f). In both cell types, we observed an increase in prenylation activity in the cytosolic lysate from cells transduced with AAV2/2-CBA-REP1 in comparison to untransduced cells or cells transduced with the AAV2/2-CBA-GFP control vector, confirming expression and functionality of the *CHM*/*REP1* transgene.

Expression of CHM/REP1 cDNA and EGFP transgenes in mouse retina

To deliver AAV vectors into the mouse retina, we used a posterior trans-scleral approach (Fig. 3a, b). To verify

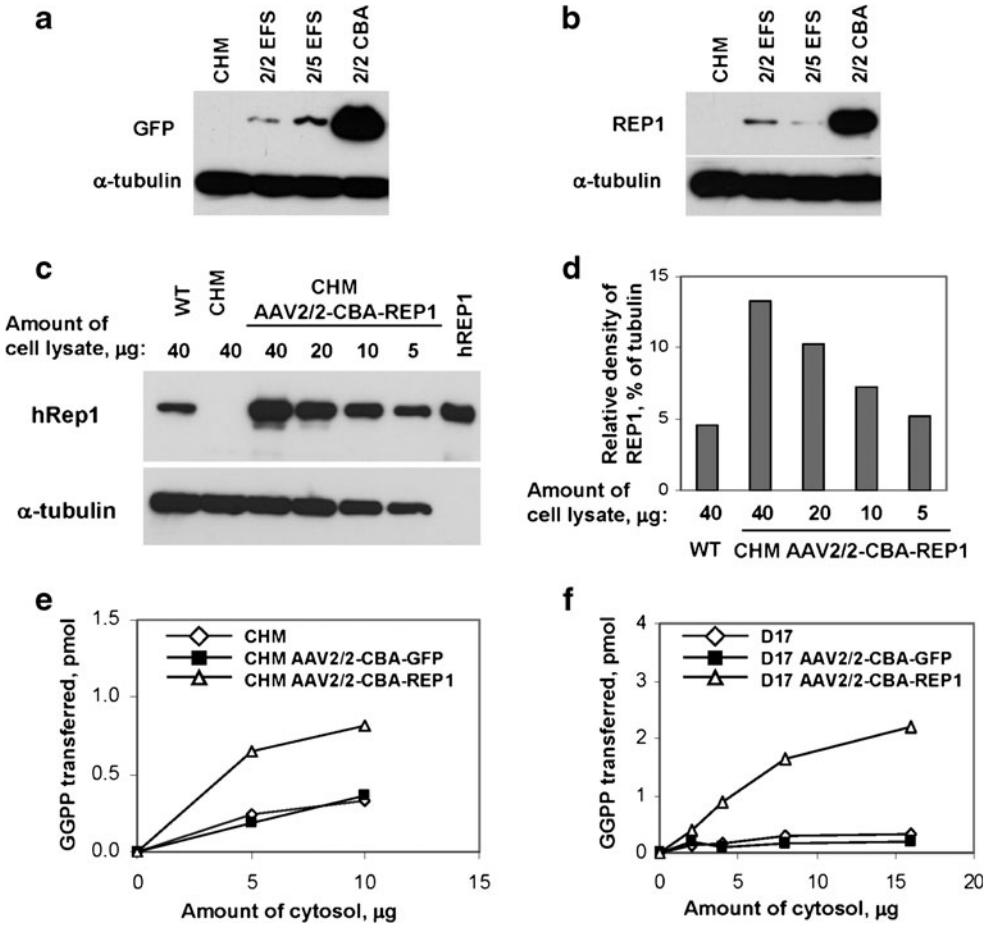

Fig. 2 **a** Immunoblot analysis of choroideremia patient fibroblasts (*CHM*) transduced with AAV2/2-EFS-GFP, AAV2/5-EFS-GFP and AAV2/2-CBA-GFP using GFP antibody and α-tubulin antibody as a loading control. Expression of GFP was analysed 7 days post-transduction. **b** Immunoblot analysis of CHM transduced with AAV2/2-EFS-REP1, AAV2/5-EFS-REP1 and AAV2/2-CBA-REP1 using 2F1 antibody and α-tubulin antibody as a loading control. Expression of REP1 was analysed 7 days post-transduction. **c** Immunoblot analysis of choroideremia patient fibroblasts that were untransduced (CHM) and transduced with AAV2/2-CBA-REP1 and control (WT) fibroblasts using 2F1 antibody and α-tubulin antibody as a loading control. Expression of REP1 was analysed 10 days post-transduction. Amount of loaded cell lysate (micrograms) is indicated *above each lane*. Recombinant human protein (hREP1) was used as a positive control. **d** Quantification of the GFP signal intensity from the western blot shown in **c** using ImageJ software. **e** In vitro prenylation analysis was performed using 5 and 20 µg of cytosolic fractions of the cell lysates isolated from untransduced (*white diamond*) and transduced with AAV2/2-CBA-GFP (*black square*) and AAV2/2-CBA-REP1 (*white triangle*) CHM fibroblasts. **f** In vitro prenylation analysis was performed using 2, 4, 8 and 16 µg of cytosolic fractions of the cell lysates isolated from untransduced D17 cell (*white diamond*) and D17 transduced with AAV2/2-CBA-GFP (*black square*) and AAV2/2-CBA-REP1 (*white triangle*)

expression of the *CHM*/*REP1* cDNA transgene in the choroideremia mouse retina, AAV2/2-EFS-REP1, AAV2/5-EFS-REP1 and AAV2/2-CBA-REP1 vectors were injected subretinally into $Chm^{null/WT}$ female carriers. The contralateral eye was not injected and served as a control. The RPE was collected 5 weeks post-injection from injected and non-injected eyes, and expression of REP1 was analysed by western blotting using 2F1 antibody, specific for human REP1. We observed a strong signal in the RPE from the eyes injected with AAV2/2-CBA-REP1 and a very faint signal after injection with AAV2/5-EFS-REP1 (Fig. 3c). These in vivo data, therefore, confirmed that AAV2/2-CBA-REP1 provided the highest level of the three tested viral vectors in the mouse RPE.

To confirm that the AAV2/2-CBA-WPRE expression cassette mediated expression in mouse photoreceptors as well as in the RPE, we injected 3–4-week-old wild-type mice with 1 µl of the AAV2/2-CBA-GFP viral vector containing 1×10^9 gp (Fig 3d–f). Within the transduced regions, we observed extensive labelling of photoreceptor cells in the outer nuclear layer in addition to labelling of the RPE, thus confirming suitability of AAV2/2-CBA-WPRE vector for transgene expression in both layers.

Expression of AAV2/2-CBA-GFP in human retinal explants

To confirm that AAV2/2-CBA-WPRE expression cassette was capable of transducing human photoreceptors in human

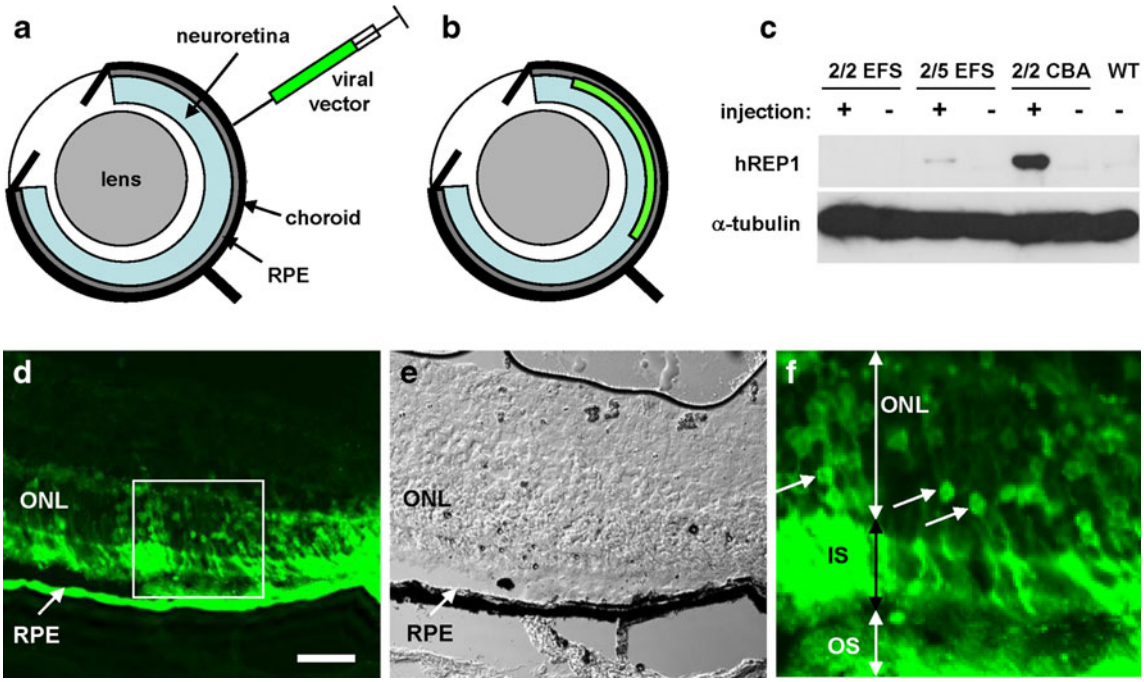

Fig. 3 **a**, **b** Illustration of delivery route for AAV viral vectors by subretinal injection. The subretinal injection was performed through posterior retina using a 10-μl Hamilton syringe and a 30° bevelled 34G needle. **c** Immunoblot analysis of RPE collected from the eyes of choroideremia mice ($Chm^{null/WT}$) injected with AAV2/2-EFS-REP1, AAV2/5-EFS-REP1 and AAV2/2-CBA-REP1 using 2F1 antibody and α-tubulin antibody as a loading control. Expression of REP1 was analysed 5 weeks post-injection. **d**–**f** Histological analysis of the AAV2/2-CBA-GFP-injected mouse eyes 5 weeks post-injection. **e** Phase contrast image corresponding to **d**. **f** Enlargement image of the area *boxed* in **d**. *Arrows* indicate nuclei of rod photoreceptors that express GFP confirming successful transduction. *RPE* retinal pigment epithelium, *ONL* outer nuclear layer, *IS* inner segments, *OS* outer segments. *Bar* is 50 μm

retina, we cultured human retinal explants ex vivo and infected them with the AAV2/2-CBA-GFP vector. Expression of the GFP transgene was assessed 11 days post-transduction. Frozen sections of explants were stained with anti-recoverin antibody and DAPI and analysed by confocal microscopy (Fig. 4). In EGFP-positive cells, we observed a strong signal with anti-recoverin antibody which confirmed transduction of photoreceptors of cultured explants.

Effects of REP1 overexpression on retinal function in wild-type mice

To examine whether REP1 overexpression might be toxic, subretinal injections of 1×10^9 gp (1 μl of undiluted suspension at 1×10^{12} gp/ml) of AAV2/2-CBA-REP1 were performed on control wild-type mice ($n=5$) at 4 weeks of age. In all cases, the contralateral eye received an equivalent dose subretinal injection of AAV2/2-CBA-GFP to act as an internal control for non-transgene-specific effects. Retinal function was assessed using ERG recording 6 months post-injection. In AAV2/2-CBA-REP1-treated eyes, clear dark-adapted ERG responses could be recorded across a 7 log unit range of flash intensity (Fig. 5a, *black lines*). Responses from AAV2/2-CBA-GFP-injected control eyes were also present across the same range, but slightly smaller in amplitude (Fig. 5a, *grey lines*). Quantification of the amplitude of the a- and b-waves of the ERG confirmed this observation (Fig. 5b). For a-wave amplitude, a two-way repeated-measures ANOVA with treatment and intensity as factors found that both were highly significant ($p<0.0001$ for both), and Bonferroni post hoc tests indicated significant pairwise differences in the three highest intensities tested (−1 to 1 log cds/m^2). For b-wave amplitude, a similar analysis (two-way repeated-measures ANOVA) also found intensity and treatment to be highly significant (both $p<0.0001$) factors, and Bonferroni post-tests revealed significant pairwise differences in all but the lowest two intensities. Despite differences in the amplitudes of both a- and b-waves, the kinetics of dark-adapted ERGs did not appear to be grossly altered (Fig. 5a). Quantification and statistical analysis of the implicit time of the a- and b-waves (Fig. 5c) found that they were not significantly different (two-way repeated-measures ANOVA with treatment and intensity as factors were $p>0.05$ in all cases).

In a related experiment, performed using a single 1-μl injection of 1:10 dilution of the viral vector (dose of 1×10^8 gp) for both AAV2/2-CBA-REP1 and AAV2/2-CBA-GFP), clear dark-adapted ERGs could again be recorded (not

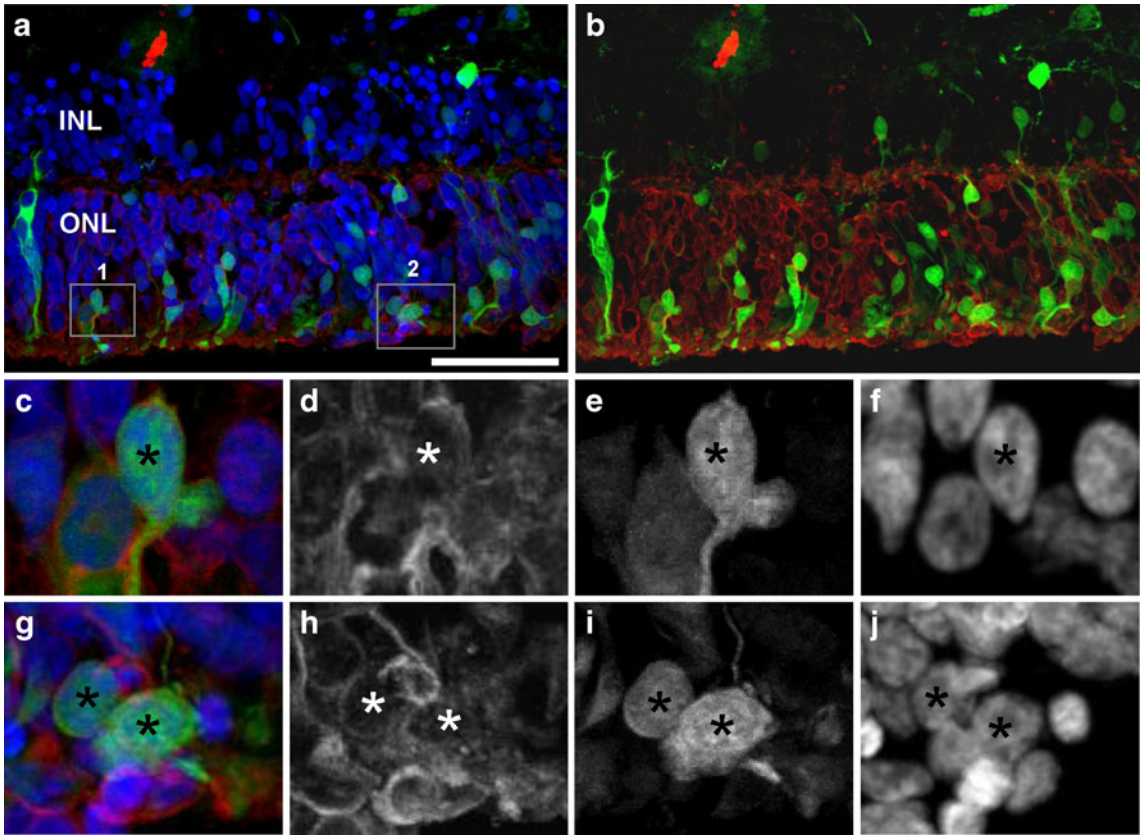

Fig. 4 Expression of pAAV2/2-CBA-GFP in human retinal explants. Explants from a 40-year-old gentleman who required retinectomy for chronic retinal detachment following endogenous Klebsiella endophthalmitis were maintained ex vivo and transduced with pAAV2/2-CBA-GFP; 11 days post-transduction explants were fixed in 4 % paraformaldehyde, cryoprotected in 20 % sucrose and frozen in OCT. Sections were stained with anti-recoverin primary and Alexa-633 secondary antibody and DAPI. **b** Merged signals for recoverin (*red*) and EGFP (*green*) are shown. **c**–**f** Enlargements of the area 1 *boxed* in **a**. **g**–**j** Enlargement of the area 2 *boxed* in **a**. **d**, **h** Recoverin-specific staining, converted to greyscale. **e**, **i** EGFP signal, converted to greyscale. **f**, **j** DAPI staining, converted to greyscale. *Asterisks* indicate cells positive for EGFP and recoverin markers. *ONL* outer nuclear layer, *INL* inner nuclear layer. *Bar* is 50 μm

shown). However, response amplitudes were now almost identical in both eyes (Fig. 5d) and very similar to those obtained after high titre AAV2/2-CBA-REP1 injections. Waveform kinetics were indistinguishable between eyes (not shown). Quantification and statistical analysis of the a- and b-wave implicit times confirmed that they were not significantly different between eyes (two-way repeated-measures ANOVA with treatment and intensity as factors were $p>0.05$ in all cases; Fig. 5e).

Light-adapted ERGs recorded in the same animals as above showed a similar pattern of results (Fig. S1). In high-dose (1×10^9 gp) AAV2/2-CBA-REP1-treated eyes, characteristic light-adapted ERG waveforms could be recorded (Fig. S1). Again, responses from high-dose (1×10^9 gp) AAV2/2-CBA-GFP-injected control eyes were present, but there was a significant reduction in b-wave amplitude (Fig. S1). As a consequence of the reduction in amplitude, responses also appeared to be slightly faster (significantly reduced b-wave implicit time). Light-adapted ERGs in low-dose (1×10^8 gp) AAV2/2-CBA-REP1-treated eyes were indistinguishable from those of low-dose (1×10^8 gp) AAV2/2-CBA-GFP-injected control eyes almost identical to those obtained after high titre AAV2/2-CBA-REP1 injection (Fig. S1).

Overall, high-dose (1×10^9 gp) or low-dose (1×10^8 gp) AAV2/2-CBA-REP1 subretinal injections did not lead to evident impairment of retinal function in wild-type mice. At the same time, responses for high-dose AAV2/2-CBA-GFP-treated eyes were reduced, suggesting that high level of GFP expression might lead to inhibitory effect on ERG responses. Hence, these experiments confirmed that no obvious toxic effects on retinal function were evident following overexpression of REP1, even at a vector dose sufficiently high to show clearly detectable toxic effects of GFP.

Effects of *REP1* overexpression on retinal function in $Chm^{null/WT}$ mice

Heterozygous female carriers ($Chm^{null/WT}$) have been shown previously to display progressive retinal degeneration with a

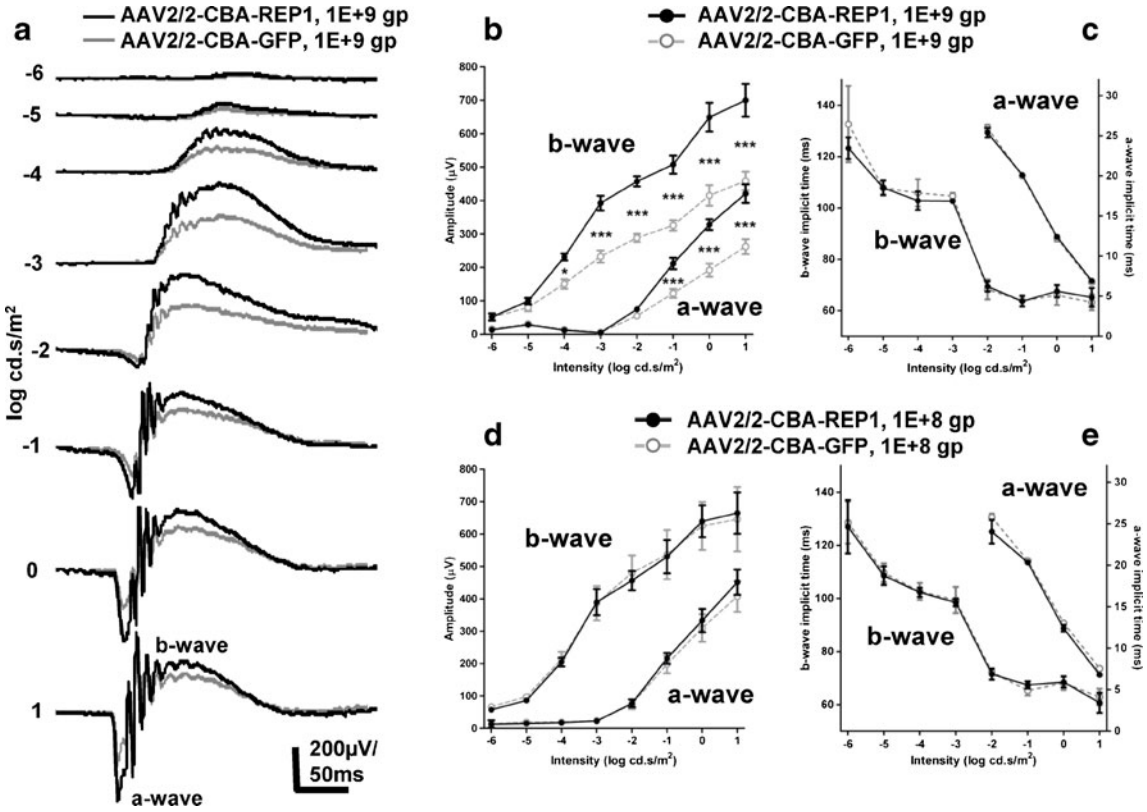

Fig. 5 ERG analysis of wild-type mice treated with AAV2/2-CBA-REP1 and AAV2/2-CBA-GFP. **a** Representative averaged ERG traces from the eyes injected with high-dose (1×10^9 gp) AAV2/2-CBA-REP1 (shown in *black*) and AAV2/2-CBA-GFP (shown in *grey*). **b**, **c** Quantification of the amplitude of a- and b-waves (**b**) and implicit time data (**c**) recorded across a range of stimulus intensities in high-dose (1×10^9 gp) AAV2/2-CBA-REP1-injected (*filled black circles* and *solid black lines*) and AAV2/2-CBA-GFP-injected (*open grey circles* and *dashed grey lines*) eyes. *Plotted symbols* show mean±SEM, $n=5$. **d**, **e** Quantification of the amplitude of a- and b-waves (**d**) and implicit time data (**e**) recorded across a range of stimulus intensities in low-dose (1×10^8 gp) AAV2/2-CBA-REP1-injected (*filled black circles* and *solid black lines*) and AAV2/2-CBA-GFP-injected (*open grey circles* and *dashed lines*) eyes. *Plotted symbols* show mean±SEM, $n=4$

clear reduction of the dark-adapted ERG amplitude [15]. To explore the potential of *CHM*/*REP1* gene therapy to ameliorate retinal function, $Chm^{null/WT}$ mice were treated with two 1-μl injections in superior and inferior areas (2 μl total) of AAV2/2-CBA-REP1 at 4 weeks of age. Subretinal injections with DMEM medium (1 μl) were performed on the contralateral eye of each animal, to act as an internal control for surgical sham effects. ERG recording was performed 6 months later, and responses were compared between vector- and sham-treated eyes. Recordings in groups that received high (2×10^9 gp, $n=5$) and low (1:10 dilution in DMEM, 2×10^8 gp, $n=5$) dose of AAV2/2-CBA-REP1 were compared to those from a contralateral sham-treated control eye in each case. In both sham- and high-dose treated eyes of $Chm^{null/WT}$ mice, intensity-dependent, dark-adapted ERG responses could be recorded (Fig. 6a). Responses from high-dose AAV2/2-CBA-REP1-treated eyes appeared to be larger in amplitude than from contralateral sham-treated eyes. Quantification of the amplitude of the a- and b-waves of the ERG supported this observation (Fig. 6b). For a-wave amplitude, a two-way repeated-measures ANOVA with treatment and intensity as factors found that both were significant ($p=0.0071$ for treatment, $p<0.0001$ for intensity). Bonferroni post-tests showed a significant ($p<0.001$) pairwise difference at the highest intensity (1 log cd s/m^2) only. For b-wave amplitude, a two-way repeated-measures ANOVA analysis found both factors to be highly significant ($p=0.0005$ for treatment, $p<0.0001$ for intensity), but Bonferroni post-tests did not indicate any significant differences in pairwise comparison at any individual intensity. Quantification of the a- and b-wave implicit times of the ERG indicated that, while there was a strong intensity dependent effect, this was not different between AAV2/2-CBA-REP1 and sham eyes (Fig. 6c).

Conversely, quantification of ERGs in $Chm^{null/WT}$ eyes treated with a lower dose (2×10^8gp) of AAV2/2-CBA-REP1 did not show improvement of the retinal function (Fig. 6d). There was a slight reduction in the amplitude of a- and b-waves compared to fellow sham-treated eyes, which could be due to a two times lower volume of sham

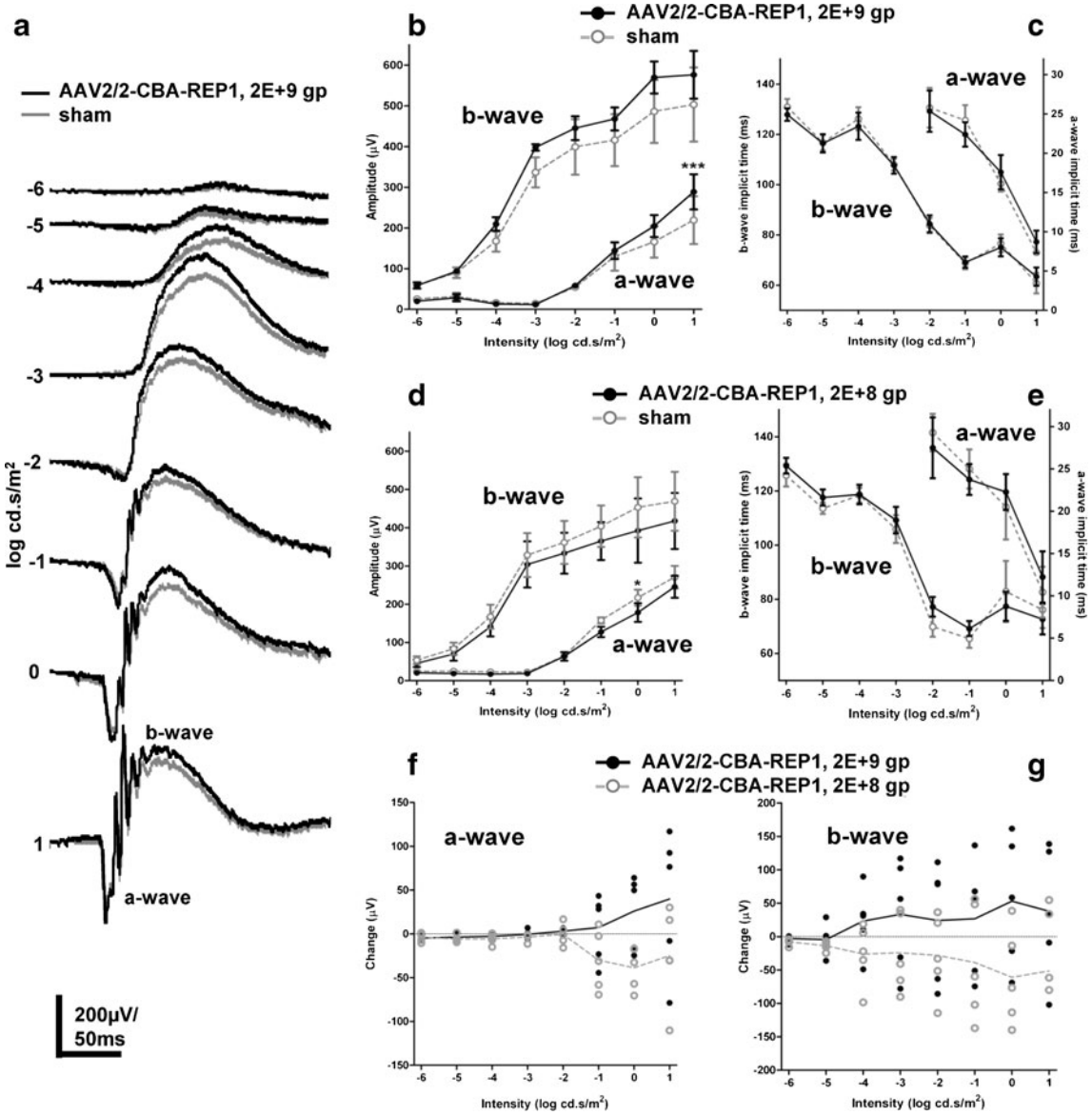

Fig. 6 ERG analysis of *Chm*$^{null/WT}$ mice, treated with AAV2/2-CBA-REP1 and DMEM (sham). **a** Representative averaged ERG traces from high-dose (2×10^9 gp) AAV2/2-CBA-REP1-injected (shown in *black*) and sham-injected (shown in *grey*) eyes. **b**, **c** Quantification of the amplitude of a- and b-waves (**b**) and implicit time data (**c**) recorded across a range of stimulus intensities in high-dose (2×10^9 gp) AAV2/2-CBA-REP1-injected (*filled black circles* and *solid black lines*) and sham-injected (*open grey circles* and *dashed lines*) eyes. *Plotted symbols* show mean±SEM, $n=5$. **d**, **e** Quantification of the amplitude of a- and b-waves (**d**) and implicit time data (**e**) recorded across a range of stimulus intensities in low-dose (2×10^8 gp) AAV2/2-CBA-REP1-injected (*filled black circles* and *solid black lines*) and sham-injected (*open grey circles* and *dashed lines*) eyes. *Plotted symbols* show mean±SEM, $n=5$. **f**, **g** Change in a-wave (**f**) and b-wave (**g**) amplitude in high-dose (2×10^9 gp, *filled black circles*) and low-dose (2×10^8 gp, *open grey circles*) AAV2/2-CBA-REP1 treatment groups. Individual values shown as point and group means as *connecting lines*

injection (1 μl) versus 2 μl for the viral injection. A two-way repeated-measures ANOVA for a-wave amplitude with treatment and intensity as factors found that both were significant ($p=0.0011$ for treatment, $p<0.0001$ for intensity). Bonferroni post-tests showed a significant ($p<0.05$) pairwise difference at 0 log cds/m^2 intensity only. For b-wave amplitude, a two-way repeated-measures ANOVA analysis found both treatment ($p=0.004$) and intensity ($p<0.0001$) to be highly significant factors, but Bonferroni post-tests did not indicate any significant differences in a pairwise comparison at any individual intensity. Quantification of the a- and b-wave implicit times of the ERG indicated that response kinetics were not different between AAV2/2-CBA-REP1 and sham eyes (Fig. 6e).

Importantly, ERG amplitudes expressed as a difference in the AAV2/2-CBA-REP1-treated eye compared to the control eye in each individual (Fig. 6f, g) illustrate improvement in the high dose (individual values and mean above zero) and reduction or no effect with low dose (values at or below zero) for both a-wave (Fig. 6f) and b-wave (Fig. 6g).

Light-adapted ERGs were recorded in most of the groups/animals above. With the exception of two individuals (where electrode stability deteriorated and they were not continued), distinct light-adapted ERG waveforms were observed (Fig. S2). However, unlike in dark-adapted ERG, no differences could be found in response amplitude between AAV2/2-CBA-REP1-injected and sham-treated eyes in either the low- or high-dose experiments (Fig. S2). A deficit in the light-adapted ERGs of *Chm*$^{null/WT}$ animals relative to wild-type controls has not been fully investigated. Consequently, a possible reason for the lack of any detectable improvement in high-dose AAV2/2-CBA-REP1-injected eyes may be the absence of an appropriate phenotype to rescue.

Therefore, a dose-related effect of AAV2/2-CBA-REP1 injection could be seen on both the a- and b-wave amplitude of dark-adapted ERGs from *Chm*$^{null/WT}$ retinas. High-dose AAV2/2-CBA-REP1 treatment appeared to improve dark-adapted retinal function in *Chm*$^{null/WT}$ mice, whereas low-dose AAV2/2-CAG-REP1 injection did not have such an effect.

Discussion

CHM would be an ideal candidate disease for gene therapy treatment due to the slow rate of degeneration and a relatively small size (1.9 kb) of the *CHM*/*REP1* coding sequence that can be used as a potential therapeutic transgene in an AAV vector. We have shown previously that in CHM, pathological changes appear in photoreceptors and RPE autonomously, and therefore, both layers need to be treated simultaneously [5]. To achieve this, we used an AAV2-based vector, which was reported to transduce both photoreceptors and RPE [14]. In comparison to the lentiviral vectors that we used in the past, AAV vectors were able to transduce RPE efficiently and were much more potent in transduction of the neuroretinal cells that were transduced with the lentiviral vectors only in the vicinity of the injection site [11, 24]. Seemingly, AAV vectors are more adept at navigating through the tightly packed area of photoreceptor outer segments, in a direction that is opposite to shedding of photoreceptor outer segments. A possible explanation of a higher penetrating ability could be a much smaller size of a mature AAV virion (20 nm), in comparison to the lentiviral particle (145 nm), that would potentially allow an AAV particle to disseminate more easily.

The ubiquitous pattern of REP1 expression provided us with the opportunity to use fibroblasts harvested from the CHM patients for the functional evaluation of the transgene expression. In future, this approach may be applied to other retinal degenerations by deriving photoreceptors in vitro via induced pluripotent stem cells [25] or transdifferentiation of the RPE [26]. In addition to dog and mouse cells, human choroideremia patient fibroblasts provided an extra species in which we could demonstrate functionality of *CHM*/*REP1* transgene expressed from our vector.

We compared two ubiquitous promoters, EFS and CBA, and found that transgene expression from CBA was higher than from EFS for both *CHM*/*REP1* and *EGFP* transgenes in human fibroblasts. One key difference between these two promoters is the inclusion of the synthetic intron in the CBA promoter upstream of the Kozak sequence at the 5′ untranslated region of the transgene. Intron processing through splicing is a feature of eukaryotic gene expression and may significantly increase viral transgene expression in certain circumstances [27]. Our data showed that CBA was a more suitable promoter to achieve a high level of transgene expression than EFS. To confirm functionality of the *CHM*/*REP1* transgene, we showed that transduction of choroideremia patient fibroblasts with AAV2/2-CBA-REP1 led to an increase in prenylation activity; a similar effect was detected in dog D17 cells transduced with AAV2/2-CBA-REP1. Thus, the AAV2/2-CBA-REP1 vector provides strong and functional transgene expression.

Although CBA is a standard ubiquitous promoter, there are cell types where it is not active, for example, cytotoxic T-lymphocytes [28]. Primate experiments to date have more commonly utilised the smaller CMV promoter in the retina [14, 29], and absolute evidence that CBA drives efficient transgene expression in human photoreceptors has been lacking. Furthermore, a safety study using CBA to drive AAV2-mediated RPE65 expression in cynomolgus monkeys failed to detect ectopic RPE65 expression in photoreceptors even with a relatively high dose of 4.5×10^{10}gp, which was unexpected [30]. In our study, to confirm that the CBA promoter can drive transgene expression in human photoreceptors, we transduced human retinal explants taken from patients undergoing retinal detachment surgery ex vivo with AAV2/2-CBA-GFP that contained an identical cassette to AAV2/2-CBA-REP1 vector. Since the retinal explants were acquired from the patients with a normal level of REP1, we decided that detection of transgene expression would be more reliably confirmed if we used an *EGFP* reporter gene as a marker of vector tropism in the human retina in place of *CHM*/*REP1* cDNA in an otherwise identical expression cassette and AAV capsid. Ideally we would wish to use CHM retinal explants; however, this was not possible due to the rarity of CHM and absence of documented retinal detachment in these patients, which might possibly be explained by firm adherence resulting from the

degeneration. This experiment confirmed excellent transduction of human photoreceptors.

Potential toxicity of REP1 overexpression was assessed by subretinal injection of wild-type mice with a high and a low dose of AAV2/2-CBA-REP1 and AAV2/2-CBA-GFP. Both dark- and light-adapted ERG responses in wild-type eyes treated with a high or a low dose of AAV2/2-CBA-REP1 were grossly normal and indistinguishable from responses from eyes injected with a low dose of AAV2/2-CBA-GFP, which suggests that AAV2/2-CBA-REP1 vector is not toxic. At the same time, ERG responses in high-dose AAV2/2-CBA-GFP-treated eyes were significantly attenuated, suggesting that a high level of GFP might be harmful to retinal cells. The mechanism of GFP toxicity may relate to an impairment of polyubiquitination [31], and hence, AAV2/2-CBA-GFP may not be a reliable control vector to gauge potential treatment effects of AAV2/2-CBA-REP1 vector on the CHM mouse ERG. For this reason, we used DMEM, which controlled for any negative effects of retinal detachment or positive sham effects of surgery in these mice. Comparison of dark-adapted ERG responses from AAV2/2-CBA-REP1- and sham-injected eyes from individual animals showed improvement of retinal function at high dose of the vector, thus demonstrating therapeutic potential of the vector.

The inclusion of a WPRE in our expression cassette is a novel development in AAV-mediated retinal gene therapy that has not been used in human retinal gene therapy clinical trials to date. It has, however, been used in other studies, such as in the AAV.GAD gene therapy study to treat Parkinson's disease [18] and has been approved by the FDA for phase II clinical trials. The inclusion of WPRE significantly enhances AAV transgene expression in the rat brain [32], in human embryonic kidney cells (HEK293) and human skin fibroblasts in vitro by up to a log unit [33]. We used a WPRE sequence previously modified to prevent expression of the viral X antigen, which has previously been linked to increased tumour susceptibility in the liver of mice [16, 34]. The advantage of using the WPRE together with an optimised promoter is that enhanced transgene expression would permit us to use a lower overall dose of AAV2 to achieve a therapeutic effect. Although one might argue that other serotypes such as AAV8 may be more efficient in targeting photoreceptors, AAV2 with the CBA promoter remains the gold standard for retinal transduction as evidenced by the sustained vision in Briard dogs treated with AAV2 vector over a decade ago [35]. Hence, valid rationale is to increase the efficiency of AAV2 through optimisation of the regulatory elements within the expression cassette, rather than changing the capsid. A combination of high therapeutic efficiency and low vector dose is particularly relevant for a disease such as CHM. Firstly, slow progression of CHM may indicate that a relatively low level of transgene expression could achieve a therapeutic effect. Secondly, low dose is particularly beneficial when transduction of other cells (cones in the case of CHM) is potentially undesirable.

In summary, our data show that AAV2/2-CBA-REP1 vector provides efficient, functional and non-toxic transgene expression in the choroideremia mouse and human cells, as well as in human and mouse RPE and photoreceptors. AAV2/2-CBA-REP1vector has a small but detectable dose-dependent therapeutic effect on retinal function in a choroideremia mouse model and thus is a suitable therapeutic agent for use in choroideremia clinical trials.

Acknowledgments This work was supported by Foundation Fighting Blindness, Fight for Sight (Tommy Salisbury Choroideremia Fund), Choroideremia Research Foundation USA, the Wellcome Trust, Health Foundation, the Royal College of Surgeons of Edinburgh, the Special Trustees of Moorfields Eye Hospital, the Oxford University Hospitals and Moorfields NIHR Biomedical Research Centres. REM and MCS are named inventors on a patent filed by the University of Oxford and including the UK Department of Health as the major stakeholder.

Conflict of interest The authors declare that they have no conflict of interests.

References

1. Heckenlively JR, Bird AJ (1988) Choroideremia. In: Heckenlively JR (ed) Retinitis pigmentosa. Lippincott, New York, pp 176–187
2. Cremers FP, van de Pol DJ, van Kerkhoff LP, Wieringa B, Ropers HH (1990) Cloning of a gene that is rearranged in patients with choroideraemia. Nature 347:674–677
3. van Bokhoven H, van den Hurk JA, Bogerd L, Philippe C, Gilgenkrantz S, de Jong P, Ropers HH, Cremers FP (1994) Cloning and characterization of the human choroideremia gene. Hum Mol Genet 3:1041–1046
4. Syed N, Smith JE, John SK, Seabra MC, Aguirre GD, Milam AH (2001) Evaluation of retinal photoreceptors and pigment epithelium in a female carrier of choroideremia. Ophthalmology 108:711–720
5. Tolmachova T, Wavre-Shapton ST, Barnard AR, MacLaren RE, Futter CE, Seabra MC (2010) Retinal pigment epithelium defects accelerate photoreceptor degeneration in cell type-specific knockout mouse models of choroideremia. Invest Ophthalmol Vis Sci 51:4913–4920
6. Hutagalung AH, Novick PJ (2011) Role of Rab GTPases in membrane traffic and cell physiology. Physiol Rev 91:119–149
7. Horgan CP, McCaffrey MW (2011) Rab GTPases and microtubule motors. Biochem Soc Trans 39:1202–1206
8. Goody RS, Rak A, Alexandrov K (2005) The structural and mechanistic basis for recycling of Rab proteins between membrane compartments. Cell Mol Life Sci 62:1657–1670
9. Cremers FP, Armstrong SA, Seabra MC, Brown MS, Goldstein JL (1994) REP-2, a Rab escort protein encoded by the choroideremia-like gene. J Biol Chem 269:2111–2117

10. MacDonald IM, Russell L, Chan CC (2009) Choroideremia: new findings from ocular pathology and review of recent literature. Surv Ophthalmol 54:401–407
11. Tolmachova T, Tolmachov OE, Wavre-Shapton ST, Tracey-White D, Futter CE, Seabra MC (2012) CHM/REP1 cDNA delivery by lentiviral vectors provides functional expression of the transgene in the retinal pigment epithelium of choroideremia mice. J Gene Med 14:158–168
12. Cideciyan AV, Aleman TS, Boye SL, Schwartz SB, Kaushal S, Roman AJ, Pang JJ, Sumaroka A, Windsor EA, Wilson JM et al (2008) Human gene therapy for RPE65 isomerase deficiency activates the retinoid cycle of vision but with slow rod kinetics. Proc Natl Acad Sci U S A 105:15112–15117
13. Jacobson SG, Cideciyan AV, Ratnakaram R, Heon E, Schwartz SB, Roman AJ, Peden MC, Aleman TS, Boye SL, Sumaroka A et al (2011) Gene therapy for Leber congenital amaurosis caused by RPE65 mutations: safety and efficacy in 15 children and adults followed up to 3 years. Arch Ophthalmol 130:9–24
14. Bennett J, Maguire AM, Cideciyan AV, Schnell M, Glover E, Anand V, Aleman TS, Chirmule N, Gupta AR, Huang Y et al (1999) Stable transgene expression in rod photoreceptors after recombinant adeno-associated virus-mediated gene transfer to monkey retina. Proc Natl Acad Sci USA 96:9920–9925
15. Tolmachova T, Anders R, Abrink M, Bugeon L, Dallman MJ, Futter CE, Ramalho JS, Tonagel F, Tanimoto N, Seeliger MW et al (2006) Independent degeneration of photoreceptors and retinal pigment epithelium in conditional knockout mouse models of choroideremia. J Clin Invest 116:386–394
16. Flajolet M, Tiollais P, Buendia MA, Fourel G (1998) Woodchuck hepatitis virus enhancer I and enhancer II are both involved in N-myc2 activation in woodchuck liver tumors. J Virol 72:6175–6180
17. Kingsman SM, Mitrophanous K, Olsen JC (2005) Potential oncogene activity of the woodchuck hepatitis post-transcriptional regulatory element (WPRE). Gene Ther 12:3–4
18. Kaplitt MG, Feigin A, Tang C, Fitzsimons HL, Mattis P, Lawlor PA, Bland RJ, Young D, Strybing K, Eidelberg D et al (2007) Safety and tolerability of gene therapy with an adeno-associated virus (AAV) borne GAD gene for Parkinson's disease: an open label, phase I trial. Lancet 369:2097–2105
19. Johnson TV, Martin KR (2008) Development and characterization of an adult retinal explant organotypic tissue culture system as an in vitro intraocular stem cell transplantation model. Invest Ophthalmol Vis Sci 49:3503–3512
20. Kostic C, Chiodini F, Salmon P, Wiznerowicz M, Deglon N, Hornfeld D, Trono D, Aebischer P, Schorderet DF, Munier FL et al (2003) Activity analysis of housekeeping promoters using self-inactivating lentiviral vector delivery into the mouse retina. Gene Ther 10:818–821
21. Beltran WA, Boye SL, Boye SE, Chiodo VA, Lewin AS, Hauswirth WW, Aguirre GD (2010) rAAV2/5 gene-targeting to rods: dose-dependent efficiency and complications associated with different promoters. Gene Ther 17:1162–1174
22. Yang GS, Schmidt M, Yan Z, Lindbloom JD, Harding TC, Donahue BA, Engelhardt JF, Kotin R, Davidson BL (2002) Virus-mediated transduction of murine retina with adeno-associated virus: effects of viral capsid and genome size. J Virol 76:7651–7660
23. Strunnikova NV, Barb J, Sergeev YV, Thiagarajasubramanian A, Silvin C, Munson PJ, Macdonald IM (2009) Loss-of-function mutations in Rab escort protein 1 (REP-1) affect intracellular transport in fibroblasts and monocytes of choroideremia patients. PLoS One 4:e8402
24. Miyoshi H, Takahashi M, Gage FH, Verma IM (1997) Stable and efficient gene transfer into the retina using an HIV-based lentiviral vector. Proc Natl Acad Sci USA 94:10319–10323
25. Comyn O, Lee E, MacLaren RE (2009) Induced pluripotent stem cell therapies for retinal disease. Curr Opin Neurol 23:4–9
26. Mao W, Yan RT, Wang SZ (2008) Reprogramming chick RPE progeny cells to differentiate towards retinal neurons by ash1. Mol Vis 14:2309–2320
27. Buchman AR, Berg P (1988) Comparison of intron-dependent and intron-independent gene expression. Mol Cell Biol 8:4395–4405
28. Barral DC, Ramalho JS, Anders R, Hume AN, Knapton HJ, Tolmachova T, Collinson LM, Goulding D, Authi KS, Seabra MC (2002) Functional redundancy of Rab27 proteins and the pathogenesis of Griscelli syndrome. J Clin Invest 110:247–257
29. Vandenberghe LH, Bell P, Maguire AM, Cearley CN, Xiao R, Calcedo R, Wang L, Castle MJ, Maguire AC, Grant R et al (2011) Dosage thresholds for AAV2 and AAV8 photoreceptor gene therapy in monkey. Sci Transl Med 3:88ra54
30. Jacobson SG, Acland GM, Aguirre GD, Aleman TS, Schwartz SB, Cideciyan AV, Zeiss CJ, Komaromy AM, Kaushal S, Roman AJ et al (2006) Safety of recombinant adeno-associated virus type 2-RPE65 vector delivered by ocular subretinal injection. Mol Ther 13:1074–1084
31. Baens M, Noels H, Broeckx V, Hagens S, Fevery S, Billiau AD, Vankelecom H, Marynen P (2006) The dark side of EGFP: defective polyubiquitination. PLoS One 1:e54
32. Paterna JC, Moccetti T, Mura A, Feldon J, Bueler H (2000) Influence of promoter and WHV post-transcriptional regulatory element on AAV-mediated transgene expression in the rat brain. Gene Ther 7:1304–1311
33. Loeb JE, Cordier WS, Harris ME, Weitzman MD, Hope TJ (1999) Enhanced expression of transgenes from adeno-associated virus vectors with the woodchuck hepatitis virus posttranscriptional regulatory element: implications for gene therapy. Hum Gene Ther 10:2295–2305
34. Themis M, Waddington SN, Schmidt M, von Kalle C, Wang Y, Al-Allaf F, Gregory LG, Nivsarkar M, Holder MV, Buckley SM et al (2005) Oncogenesis following delivery of a nonprimate lentiviral gene therapy vector to fetal and neonatal mice. Mol Ther 12:763–771
35. Bennicelli J, Wright JF, Komaromy A, Jacobs JB, Hauck B, Zelenaia O, Mingozzi F, Hui D, Chung D, Rex TS et al (2008) Reversal of blindness in animal models of Leber congenital amaurosis using optimized AAV2-mediated gene transfer. Mol Ther 16:458–465